

Geophysical Research Letters®



RESEARCH LETTER

10.1029/2023GL105205

Key Points:

- Spaceborne Solar-Induced Fluorescence (SIF) data was used to analyze soil moisture-related vegetation stress regimes in northern peatlands
- For most locations, waterlogging as well as drought stress regimes occurred and alternated depending on peatland water level dynamics
- The SIF-based stress response observations are supported by in situ data of Gross Primary Production

Supporting Information:

Supporting Information may be found in the online version of this article.

Correspondence to:

M. Bechtold,
michel.bechtold@kuleuven.be

Citation:

Valkenborg, B., De Lannoy, G. J. M., Gruber, A., Miralles, D. G., Köhler, P., Frankenberg, C., et al. (2023). Drought and waterlogging stress regimes in northern peatlands detected through satellite retrieved solar-induced chlorophyll fluorescence. *Geophysical Research Letters*, 50, e2023GL105205. <https://doi.org/10.1029/2023GL105205>

Received 3 JUL 2023
Accepted 15 SEP 2023

Author Contributions:











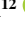


Conceptualization: Bram Valkenborg, Gabriëlle J. M. De Lannoy, Ankur R. Desai, Eeva-Stiina Tuittila, Michel Bechtold

Data curation: Philipp Köhler, Christian Frankenberg, Ankur R. Desai, Elyn Humphreys, Janina Klatt, Annalea Lohila, Mats B. Nilsson, Eeva-Stiina Tuittila, Michel Bechtold

Formal analysis: Bram Valkenborg, Michel Bechtold

Funding acquisition: Gabriëlle J. M. De Lannoy

Drought and Waterlogging Stress Regimes in Northern Peatlands Detected Through Satellite Retrieved Solar-Induced Chlorophyll Fluorescence

Bram Valkenborg¹ , Gabriëlle J. M. De Lannoy¹ , Alexander Gruber^{1,2} , Diego G. Miralles³ , Philipp Köhler^{4,5} , Christian Frankenberg^{4,6} , Ankur R. Desai⁷ , Elyn Humphreys⁸ , Janina Klatt⁹ , Annalea Lohila^{10,11} , Mats B. Nilsson¹² , Eeva-Stiina Tuittila¹³ , and Michel Bechtold¹ 

¹Department of Earth and Environmental Sciences, KU Leuven, Leuven, Belgium, ²Department of Geodesy and Geoinformation, Technische Universität Wien (TU Wien), Vienna, Austria, ³Hydro-Climate Extremes Lab (H-CEL), Ghent University, Ghent, Belgium, ⁴Division of Geological and Planetary Sciences, California Institute of Technology, Pasadena, CA, USA, ⁵Remote Sensing and Products Division at EUMETSAT, Darmstadt, Germany, ⁶Jet Propulsion Laboratory, California Institute of Technology, Pasadena, CA, USA, ⁷Department of Atmospheric and Oceanic Sciences, University of Wisconsin-Madison, Madison, WI, USA, ⁸Department of Geography and Environmental Studies, Carleton University, Ottawa, ON, Canada, ⁹Peatland Science Centre (PSC), University of Applied Sciences Weihenstephan-Triesdorf, Freising, Germany, ¹⁰Finnish Meteorological Institute, Climate System Research, Helsinki, Finland, ¹¹Faculty of Science, University of Helsinki, Institute for Atmospheric and Earth System Research (INAR)/Physics, Helsinki, Finland, ¹²Department of Forest Ecology and Management, Swedish University of Agricultural Sciences, Umea, Sweden, ¹³School of Forest Sciences, University of Eastern Finland, Joensuu, Finland

Abstract The water table depth (WTD) in peatlands determines the soil carbon decomposition rate and influences vegetation growth, hence the above-ground carbon assimilation. Here, we used satellite-observed Solar-Induced chlorophyll Fluorescence (SIF) as a proxy of Gross Primary Production (GPP) to investigate water-related vegetation stress over northern peatlands. A linear model with interaction effects was used to relate short- and long-term anomalies in SIF with WTD anomalies and the absolute WTD. Most locations showed the occurrence of drought and waterlogging stress though regions with exclusively waterlogging or drought stress were also detected. As a spatial median, minimal water-related vegetation stress was found for a WTD of -0.22 m (short-term) and -0.20 m (long-term) (± 0.01 m, 95% confidence interval of statistical uncertainty). The stress response observed with SIF is supported by an analysis of in situ GPP data. Our findings provide insight into how changes in WTD of northern peatlands could affect GPP under climate change.

Plain Language Summary Water table depth is an important variable influencing the carbon cycle and vegetation growth in northern peatlands. In this paper, the impact of changing wetness conditions on vegetation growth over peatlands was studied through satellite measurements of solar-induced fluorescence (SIF), which is a radiation signal emitted by vegetation during photosynthesis. Previous studies over ecosystems on mineral soil, that is, not over peatland, suggested a response of SIF to drought conditions. In our study, it was shown that peatland vegetation experiences moisture-related growth stress under both very wet and very dry conditions, which might reduce the photosynthesis efficiency and the ability to capture and store CO₂. Stress due to drought conditions was detected for peatlands in the south of the Western Siberian Lowlands and the Boreal Plains. Stress due to prolonged wet conditions occurred for example, in the north of the Western Siberian Lowlands and the north of the Hudson Bay Lowlands.

1. Introduction

Peatlands are wetlands that contain 30% or more accumulated decomposed organic material in the surface soil layer with a minimum thickness of 30 cm (Joosten & Clarke, 2002; Limpens et al., 2008). Wet conditions are necessary to ensure the continuing accumulation of dead plant material by limiting aerobic decomposition (Clymo et al., 1998; Gallego-Sala et al., 2018). Therefore, disturbances such as droughts may pose a threat to both the water and carbon balance in peatlands (Helbig et al., 2020; Rinne et al., 2020; Waddington et al., 2014). Even though a long-term lowering of the water table depth (WTD) would most likely increase aerobic peat

© 2023. The Authors.

This is an open access article under the terms of the [Creative Commons Attribution License](https://creativecommons.org/licenses/by/4.0/), which permits use, distribution and reproduction in any medium, provided the original work is properly cited.

Investigation: Bram Valkenborg, Alexander Gruber, Ankur R. Desai, Eeva-Stiina Tuittila, Michel Bechtold
Methodology: Bram Valkenborg, Gabriëlle J. M. De Lannoy, Alexander Gruber, Diego G. Miralles, Philipp Köhler, Christian Frankenberg, Ankur R. Desai, Eeva-Stiina Tuittila, Michel Bechtold
Supervision: Bram Valkenborg, Gabriëlle J. M. De Lannoy, Ankur R. Desai, Eeva-Stiina Tuittila, Michel Bechtold
Validation: Bram Valkenborg, Ankur R. Desai, Elyn Humphreys, Janina Klatt, Annalea Lohila, Mats B. Nilsson, Eeva-Stiina Tuittila, Michel Bechtold
Visualization: Bram Valkenborg
Writing – original draft: Bram Valkenborg
Writing – review & editing: Gabriëlle J. M. De Lannoy, Alexander Gruber, Diego G. Miralles, Philipp Köhler, Christian Frankenberg, Ankur R. Desai, Elyn Humphreys, Janina Klatt, Annalea Lohila, Mats B. Nilsson, Eeva-Stiina Tuittila, Michel Bechtold

decomposition, and thus also the CO₂ flux from the soil to the atmosphere (Fenner & Freeman, 2011), it may also result in a higher gross primary production (GPP) when vegetation adapts to the new conditions. The resulting net effect on the carbon budget is unclear (Loisel et al., 2021; Moore, 2002). Similarly, short-term variations in WTD also influence vegetation growth and above-ground carbon uptake, as well as below-ground carbon processes (Waddington et al., 2014).

Satellite retrievals of Solar-Induced Fluorescence (SIF) provide a new opportunity to investigate the response of GPP to soil moisture (Jonard et al., 2020; Wang et al., 2021) and possibly WTD variations. SIF is emitted by excited chlorophyll molecules after absorption of light (Lees et al., 2018; Mohammed et al., 2019). SIF, as a proxy of photosynthesis (Baker, 2008), is strongly related to GPP (Frankenberg et al., 2011; Guanter et al., 2012). Several studies reported a decline in SIF due to environmental stress (Panigada et al., 2014; Sun et al., 2015; Wieneke et al., 2018). Sun et al. (2015), for example, showed that negative soil moisture anomalies (droughts) led to negative anomalies in SIF for non-peatland areas. Peatlands might additionally exhibit a stress behavior—with an anomalously low SIF—during excessively wet conditions that frequently occur in peatlands.

While thermal and multispectral satellite data were successfully used for detecting plant water stress during drought conditions (Brown et al., 2008; Harris, 2008; Wardlow et al., 2012), those signals are difficult to interpret during waterlogging conditions. The high water content causes strong alterations to the thermal properties and reflectance that are not related to vegetation stress (Worrall et al., 2019). Furthermore, the Normalized Difference Vegetation Index and other optical indices related to plant biomass have time lags in response to stress (Tian et al., 2019; Walther et al., 2018) while SIF more directly reflects stress-induced changes in photosynthesis. Several studies showed that *Sphagnum mosses*, a prominent plant genus across peatlands, react with a decline in photosynthesis both at the dry and wet edge of a typical moisture range for peatlands by measuring CO₂ gas exchange (Robroek et al., 2009; Schipperges & Rydin, 1998) or by assessing photosynthetic efficiency at the leaf level through the pulse-amplitude-modulation chlorophyll fluorescence method (Harris, 2008; Van Gaalen et al., 2007). These findings encourage the use of SIF for studying water-related vegetation stress in peatlands. However, it is important to exercise caution in interpreting the results due to the distinct nature of the measurements (active vs. passive, leaf scale vs. landscape scale).

In this study, the temporal behavior of SIF was related to WTD variations at a large scale over peatlands of the Northern Hemisphere for the first time. More specifically, it was hypothesized that the relationship between SIF anomalies (SIF_{n,anom}) and WTD anomalies (WTD_{anom}) depends upon WTD.

2. Methodology

2.1. Data Sources

This study used SIF retrievals from the TROPOMI sensor on board Sentinel-5P, which collects data at a spatial resolution of 7 km along-track to 3.5–7 km across-track and a daily temporal resolution (Köhler et al., 2018). The analysis was performed on far-red SIF at 740 nm. Various quality control measures were applied in the retrieval, including the removal of outliers by a χ^2 -test and the removal of view zenith angles larger than 60°. Furthermore, SIF was daily corrected to account for the large swath width of Sentinel-5P which covers multiple time zones (Köhler et al., 2018).

SIF emitted by excited chlorophyll molecules is largely influenced by Photosynthetic Active Radiation (PAR). To allow isolating the relationship between SIF and WTD, the effect of varying incoming radiation over space and time was eliminated by normalizing SIF (Wm⁻² sr⁻¹ μm⁻¹) by PAR (Wm⁻²):

$$\text{SIF}_n = \frac{\text{SIF}}{\text{PAR}} \quad (1)$$

where SIF_n (sr⁻¹ μm⁻¹) is the normalized SIF. PAR data were taken from the Clouds and the Earth's Radiant Energy System (CERES) project (Doelling et al., 2013, 2016) and were available on a 1° × 1° grid at an hourly resolution. The total PAR was computed as the sum of diffuse and direct radiation. The PAR measurements were temporally matched to the SIF measurements by linear interpolation.

In peatlands, root-zone soil moisture conditions are closely linked to WTD due to the generally shallow water table (Burdun et al., 2020). Therefore, WTD was taken as a proxy to describe plant water availability in a peatland.

Regional WTD estimates were obtained from a data assimilation product in which L-band brightness temperature observations from the Soil Moisture Ocean Salinity were assimilated into the NASA Catchment Land Surface Model that included peatland-specific routines (PEATCLSM, (Bechtold et al., 2019, 2020)). The WTD estimates, here defined as negative below ground, were available at a 9 km and daily resolution.

2.2. Data Preparation

All data sets were harmonized to an 8-day, $0.2^\circ \times 0.2^\circ$ resolution for the period from 2018 through 2021. The regridding was based on averaging the finer-resolution SIF and WTD data to 0.2° . Before averaging, SIF measurements for which the cloud fraction was larger than 0.7, were masked out. We applied a rather relaxed cloud filter in combination with a normalization by PAR to derive a good temporal coverage as suggested by Guanter et al. (2021). Regridding to a coarser resolution mitigated the noise in the SIF data. PAR data were processed through first-order conservative remapping. Only the Northern Hemisphere growing season from June through September was taken into account, resulting in a maximum of $N = 15$ data points per pixel per growing season.

Additional masking was applied to the aggregated data. First, data during frozen soil conditions as indicated by PEATCLSM simulations were masked out using a topsoil temperature threshold of 4°C , which is well above 0°C to account for possible model errors in freeze-thaw estimation (Gruber et al., 2020). Second, only pixels with a peat fraction larger than 0.5 according to Reichle et al. (2023) were kept for the analysis.

2.3. Anomalies for Stress Detection

When a non-stressed reference state or flux is difficult to derive, anomalies in vegetation and soil moisture time series can be used to monitor drought impacts on ecosystems (AghaKouchak et al., 2015; Nanzad et al., 2019; Sun et al., 2015; Wardlow et al., 2012). While in previous literature on stress detection anomalies were typically calculated with respect to the climatology, in our study, we split up the anomalies into a high- and a low-frequency signal (Draper & Reichle, 2015; Gruber & Reichle, 2022). Short-term anomalies were calculated as the difference between the 8-day averaged data and the seasonality, whereas long-term anomalies were calculated as the deviations of the seasonality from the climatology. The seasonality was obtained by running a 5-week moving-average window over the data in each year, and the climatology was defined as the average of the seasonality on each day of the year over all 4 years.

We propose the use of short-term anomalies as an approach to analyze the immediate response of the current vegetation to WTD changes. It follows the basic idea of relating the change in one variable between two successive time steps to the change in another variable. By using short-term anomalies instead of simple differences, the confounding effect of long-term gradual changes (e.g., the seasonal phenological cycle) is minimized through the removal of the current seasonality (Gruber & Reichle, 2022). In contrast, long-term anomalies allow analyzing a possible vegetation response to interannual variability of soil moisture conditions and also include lagged effects of stress due to altered vegetation development (Lund et al., 2012).

2.4. WTD Stress Model

Figure 1 illustrates our hypothesis that the sign of the relationship between $\text{SIF}_{n,\text{anom}}$ and WTD_{anom} depends on the WTD state itself. Amid the growing season, where WTDs are typically deep, it is expected that anomalously deep WTDs (i.e., negative WTD_{anom}), cause anomalously low SIF due to enhanced drought stress (state 4 in Figure 1). In contrast, early or late in the growing season, when WTDs are usually shallow, negative WTD_{anom} are expected to cause positive $\text{SIF}_{n,\text{anom}}$ by mitigating waterlogging stress (state 2 in Figure 1). Likewise, positive WTD_{anom} at shallow WTDs will further increase waterlogging stress (state 1 in Figure 1), whereas positive WTD_{anom} at deep WTDs will mitigate drought stress (state 3 in Figure 1). Put simply, we expect a negative relationship between WTD_{anom} and $\text{SIF}_{n,\text{anom}}$ at shallow WTDs and a positive relationship at deep WTDs. At each pixel, this temporal relationship was approximated by a linear model with an interaction effect, hereinafter referred to as the WTD stress model:

$$\text{SIF}_{n,\text{anom}} = (\alpha + \beta \text{WTD})\text{WTD}_{\text{anom}} \quad (2)$$

in which α ($\text{sr}^{-1}\text{m}^{-2}$) and β ($\text{sr}^{-1}\text{m}^{-3}$) are fitting parameters. α represents the slope of the graph in Figure 1c at $\text{WTD} = 0$ m. In PEATCLSM, $\text{WTD} = 0$ m is the maximum WTD and represents a state at which half of the

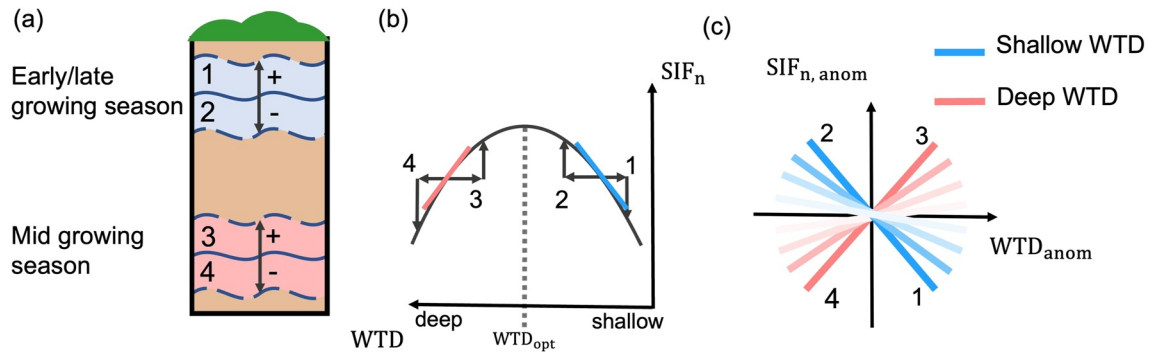


Figure 1. (a) Illustration of a peat soil profile with a shallow water table depth (WTD) in the early and late growing season, and a deep WTD in the middle of the growing season. The dashed lines indicate positive or negative anomalies for (state 1 or 2) shallow and (state 3 or 4) deep WTDs. (b) Illustration of the hypothesized relation between SIF_n and WTD. State 1 and 4 describe an increase in stress, that is, lower SIF_n , states 2 and 3 describe a decrease in stress, that is, higher SIF_n . (c) Illustration of the used stress model: for deep WTDs a positive relationship between $SIF_{n,anom}$ and WTD_{anom} is expected, for shallow WTDs a negative relationship is expected. At WTD_{opt} , it is $SIF_{n,anom} = 0$ for any WTD_{anom} .

peatland microrelief is flooded. α would be negative (= waterlogging regime) if our hypothesis held true. If $WTD < 0$ m, then the slope of the $SIF_{n,anom}$ versus WTD_{anom} relationship equals to $\alpha + \beta WTD$, that is, it changes with WTD. This change is proportional to β , which ought to be negative to reduce the slope from negative to positive when moving from shallow (e.g., -0.05 m) to deep (e.g., -0.5 m) WTD (move from right to left on Figure 1b).

Resulting from Equation 2, the optimal WTD (WTD_{opt}) at which no drought or waterlogging stress occurs, that is, when a non-zero WTD_{anom} results into a zero $SIF_{n,anom}$, is:

$$WTD_{opt} = -\frac{\alpha}{\beta} \quad (3)$$

If the above-described moisture-related stress response behavior would indeed hold and the WTD range at a particular location covered sufficiently dry and wet conditions during the study period, WTD_{opt} , calculated by Equation 3, ought to be found between the deepest and shallowest WTD.

We estimated the linear coefficients α and β of Equation 2 by minimizing the sum of the total squared error between modeled and observed $SIF_{n,anom}$ at each peatland pixel, separately for short- and long-term anomalies, and without imposing any constraints on the coefficients. Thereafter, we verified whether the fitted model Equation 2 met our hypothesis or not. This was done based on an evaluation of (a) the regressed α and β , (b) the predicted WTD_{opt} and (c) the significance of the temporal fit in terms of the coefficient of determination (R^2), for all pixels in the domain, individually. The significance of the fits was calculated based on the F -test for which a significance threshold of $p < 0.05$ was applied and the sample size was corrected for temporal autocorrelation. We further used the WTD stress model Equation 2 to estimate the percentage of waterlogging and drought regime days for each pixel. Timesteps for which $\alpha + \beta WTD$ in Equation 2 was negative were considered a waterlogging regime, timesteps for which $\alpha + \beta WTD$ were positive were considered a drought stress regime.

2.5. Validation of Modeling Approach at Eddy Covariance Flux Towers

Due to the lack of in situ measurements of SIF in peatlands, it is not possible to directly validate the calibrated models. However, there exists a strong positive relationship between SIF and GPP (Guanter et al., 2014; Sun et al., 2017), and the link of in situ GPP signals with WTD could thus serve as a validation of our model with satellite-based SIF. Unfortunately, GPP from Eddy Covariance (EC) flux towers is only available in areas with peatlands intermixed by upland forest soils or other land covers, and those grid cells were masked based on our peat fraction threshold. Thus a comparison at pixel level was not possible.

Despite these limitations, we fitted the proposed WTD stress model to GPP data from six different flux towers in northern peatlands with at least 4 years of overlapping in situ GPP, PAR, and WTD data (see Table S1 in Supporting Information S1 for the site overview). Similar to the SIF data, 30-min GPP data (without gap filling) was

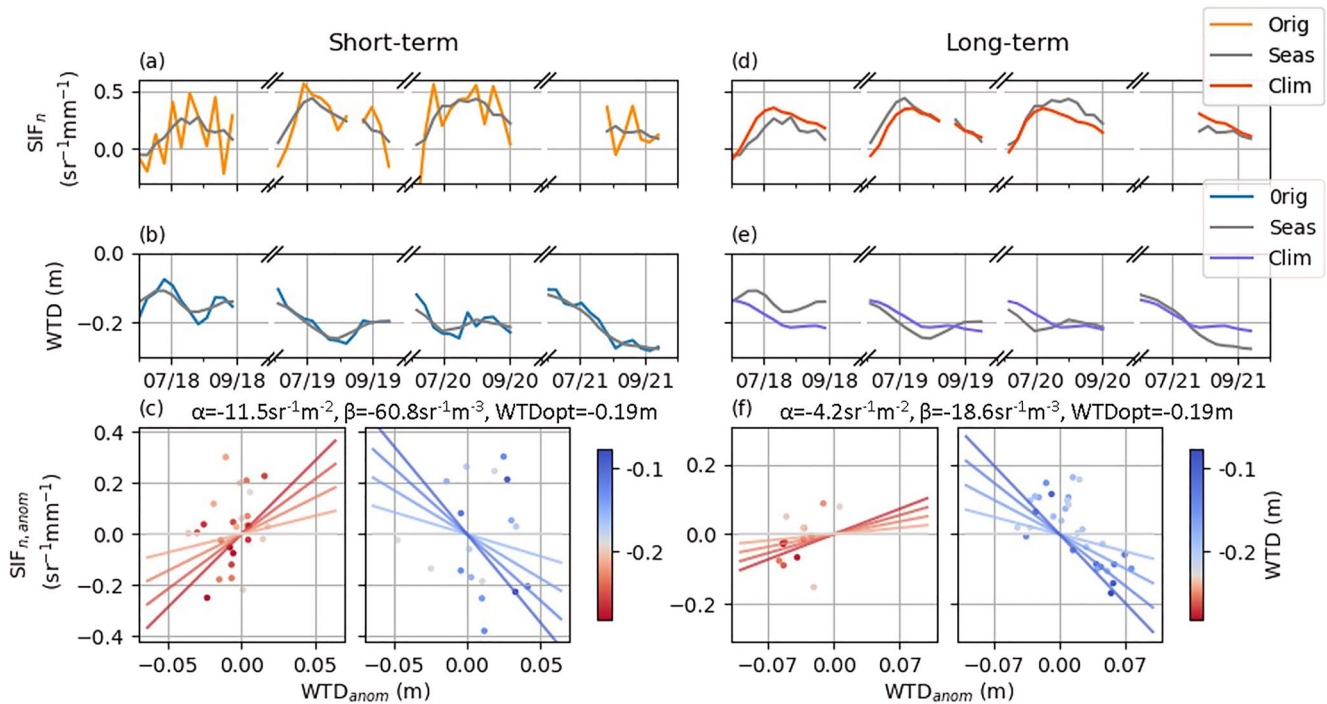


Figure 2. Time series for an example pixel (52.3°N , 85.5°W) of (a) SIF_n and its seasonality (Seas), (b) same for water table depth (WTD), (d) SIF_n seasonality and climatology (Clim), and (e) same for WTD. For this pixel, the WTD stress model was calibrated for (c) short-term anomalies and (f) long-term anomalies of SIF_n and WTD. The fitted surface is visualized by the different lines in two panels (left: $\text{WTD} \leq \text{WTD}_{\text{opt}}$, right: $\text{WTD} \geq \text{WTD}_{\text{opt}}$), and crosses $\text{SIF}_{n,\text{anom}} = 0$ (lightest color) when $\text{WTD}_{\text{opt,st}} = -0.19$ m or $\text{WTD}_{\text{opt,lt}} = -0.23$ m, for short- and long-term anomalies, respectively. The gray zones of the colorbars are centered around the respective WTD_{opt} .

temporally aggregated to 8-day averages, and was normalized by locally measured PAR (also 8-day aggregated after cross-masking with 30-min GPP data) prior to the calculation of anomaly time series. Similar results for the calibrated WTD stress model (Equation 2) with in situ $\text{GPP}_{n,\text{anom}}$ and satellite-based $\text{SIF}_{n,\text{anom}}$, would validate the underlying WTD stress model assumptions.

3. Results and Discussion

3.1. Detection of Waterlogging and Drought Stress Regimes

Figure 2a–2e shows example time series of SIF_n and WTD together with their seasonality and climatology at a single pixel. SIF_n scales out the direct influence of PAR but seasonal trends remain, which are explained by changing photosynthetically active biomass. We did not additionally normalize SIF_n by a biomass proxy as is done, for example, with fractional PAR, NIRv or NIRvP (R. Qiu et al., 2022b; Dechant et al., 2022), due to the high sensitivity of optical vegetation indices to seasonally varying vegetation composition and water fraction in peatlands (Ji et al., 2009; Walther et al., 2018). Instead, we based our analysis of water-related stress fully on anomalies, which minimizes the effects of the remaining seasonal cycle.

Anomalously shallow WTD occurred at the beginning of the growing season of 2020 (Figure 2b). Around that same period, SIF_n was also lower than its seasonality, suggesting a waterlogging stress response (i.e., a negative short-term $\text{SIF}_{n,\text{anom}}$). One of the deepest WTDs occurred in September 2021 when WTD dropped to -0.28 m. For this period, the seasonalities of WTD and SIF_n also dropped below the climatology, suggesting that the apparent drought stress persisted over a considerable amount of time (i.e., negative long-term $\text{SIF}_{n,\text{anom}}$). In contrast, the growing season of 2018 was an exceptionally wet period with the WTD (seasonality) continuously being above the climatological average (Figure 2e). During the same period, the SIF seasonality was consistently lower than its climatology, suggesting waterlogging stress.

Figures 2c and 2f show $\text{SIF}_{n,\text{anom}}$ and WTD_{anom} at different WTD levels, separately for WTDs below and above WTD_{opt} , and for short- and long-term anomalies, respectively. Also shown, is the fitted WTD stress model

(Equation 2) and the corresponding parameters. Although R^2 values were rather low ($R_{st}^2 = 0.14$, $R_{lt}^2 = 0.35$, $N = 60$), the fitted WTD stress model behaved as hypothesized (Section 1 and Figure 1), that is, it exhibited a negative slope at shallow WTDs and a positive slope at deep WTDs with a WTD_{opt} within the natural WTD range at that pixel. This behavior is seen for both short-term and long-term anomalies, but is most prominent for the long-term anomalies which show a distinct negative relationship between $SIF_{n,anom}$ and WTD_{anom} for shallow WTD due to waterlogging. The change in sign in the relationship between $SIF_{n,anom}$ and WTD_{anom} is characteristic for northern peatlands and had not been observed over mineral soils, where the sign of this relationship usually remains positive (Sun et al., 2015).

Note that our WTD stress model estimated only a single WTD level, WTD_{opt} , at which SIF is insensitive to WTD anomalies (i.e., “moisture-related stress-free” conditions). In reality, however, there might be a range of WTDs for which plants experience optimal growing conditions. However, the limited amount and rather low quality of available SIF observations were insufficient to properly fit a more complex model that might be able to accurately account for this behavior.

As a validation of the WTD stress model, Figure 3 shows the results of fitting the WTD stress model to the in situ GPP data. For the short-term anomalies, fitted models align with the hypothesis for five of the six sites (i.e., not for site US_LOS). While the individual fits were not significant, a single fit to the short-term anomalies of all sites resulted in a significant fit ($p = 0.02$) in line with the hypothesis. For the long-term anomalies, the stress model only identified waterlogging stress for one site with high annual precipitation (site DE_SFS, Table S1 in Supporting Information S1) whereas all other sites were dominated by drought stress with only minor WTD-dependent modulation of the $SIF_{n,anom}$ to $WTD_{n,anom}$ relationship. For those model fits, WTD_{opt} lies outside the observed WTD range and cannot be interpreted as optimal WTD. Interestingly, the observed difference between short-term and long-term results regionally agrees with SIF-based results (see Section 3.2).

The application of the WTD stress model to in situ GPP data indicates that waterlogging stress might be more directly detectable in short-term anomalies. In contrast, long-term anomalies do not only reflect instantaneous stress reactions but also include time-lag effects. The latter is supported by Lund et al. (2012) who reported that peatlands are more sensitive to drought impacts during leaf-out and canopy development than during the full canopy stage, and that early season droughts result in anomalies later in the season. At the same time, our results based on the short-term SIF anomalies should be considered with caution. Recent findings indicate a weakening of the strong positive fluorescence-GPP relationship at canopy scale during short-term drought events for a deciduous tree species (Helm et al., 2020) and even an inversion of the fluorescence-GPP relationship during an extreme heat wave at both the canopy and leaf scales for evergreen broadleaved trees (Martini et al., 2022). Future research should establish a better understanding of leaf-level mechanisms under stress conditions and the related fluorescence signal measured at the canopy scale also for peatland ecosystems.

3.2. Spatial Evaluation of the WTD Stress Model

Figure 4 shows the frequency distribution of α , β , WTD_{opt} and R^2 for short- and long-term anomalies. It is acknowledged that there are many more pixels with a non-significant fit than with a significant fit, which results from our simple model with a single variable, the high data noise, and the limited time period. Still, the abundance of pixels supports a valid interpretation.

For the majority of the pixels, α and β values were negative, that is, according to the hypothesis (of significant fits: $\alpha = 76\%$, $\beta = 64\%$ (short-term), $\alpha = 95\%$, $\beta = 42\%$ (long-term); of non-significant fits: $\alpha = 60\%$, $\beta = 55\%$ (short-term), $\alpha = 54\%$, $\beta = 54\%$ (long-term), see Figure 4). The median of all WTD_{opt} was -0.22 m for the short-term and -0.20 m for the long-term analysis. To estimate the 95% confidence intervals of these median values, we fitted the model at each pixel 100 times using bootstrapped samples. The fits were then used to calculate 100 times the spatial median of WTD_{opt} . The resulting 95% confidence intervals of the median values were determined to be ± 0.01 in both cases. This value represents the statistical uncertainty and does not include any possible systematic uncertainties for example, related to a bias in WTD from PEATCLSM which can regionally reach about ± 0.1 m (Bechtold et al., 2019).

For most pixels, the WTD_{opt} estimates were between the minimum and the maximum WTD for the short-term (significant: 55%, non-significant: 60%) analysis but not for the long-term (significant: 16%, non-significant: 45%) analysis (see Figure 1b). This has similarly been observed for the in situ GPP data and may indicate the

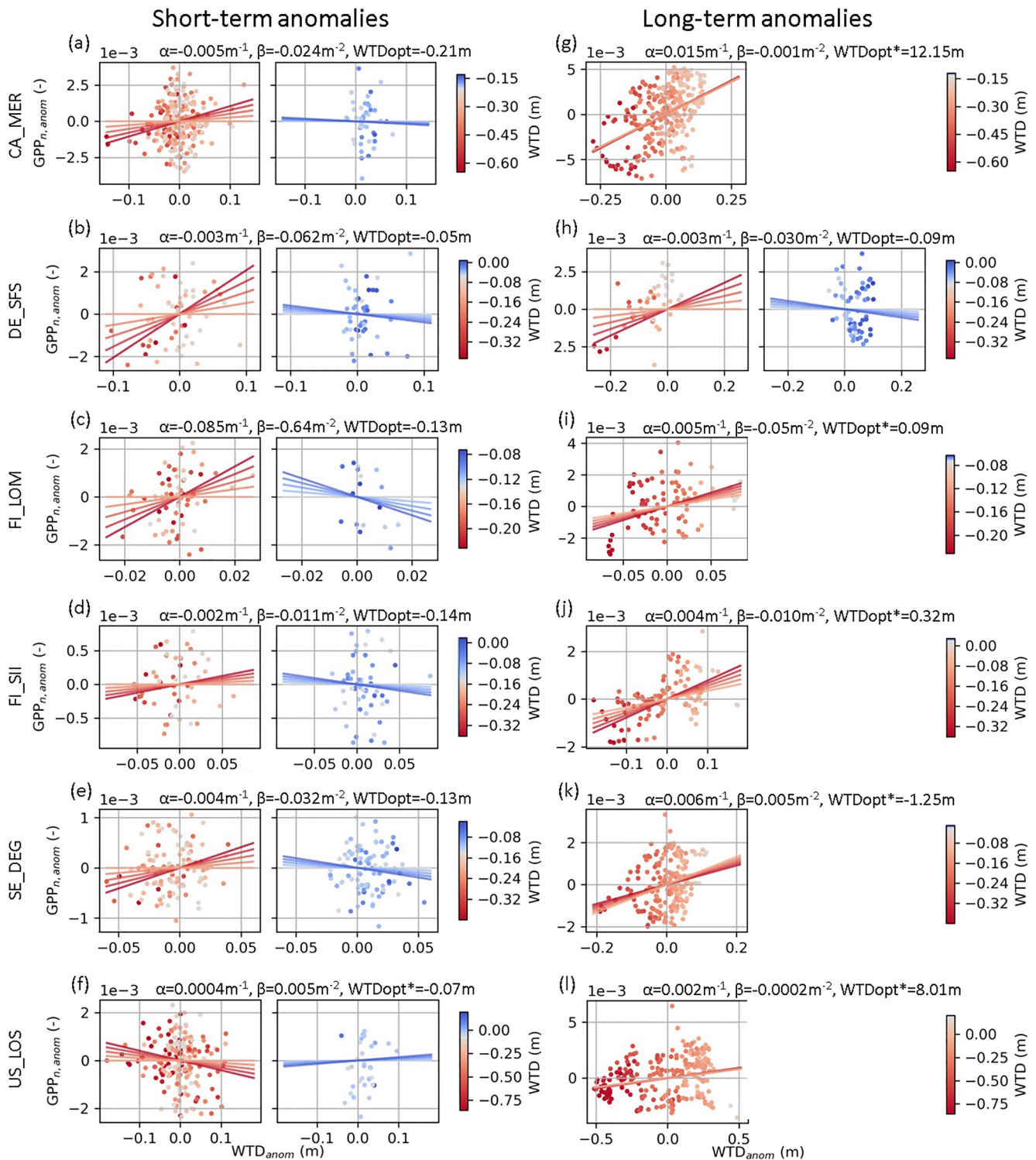


Figure 3. Similar to Figures 2c and 2f but with the water table depth (WTD) stress model fitted to Gross Primary Production data from six eddy covariance sites for (a to f) short-term anomalies and (g to l) long-term anomalies. Parameter values are indicated at the top of each subplot. WTD_{opt} values marked with an asterisk cannot be interpreted as optimal WTD because either the model fit did not correspond to the model hypothesis (US_LOS, short-term) or an optimal WTD was fitted outside of the observed WTD range and only drought stress was detected (five of six sites, long-term).

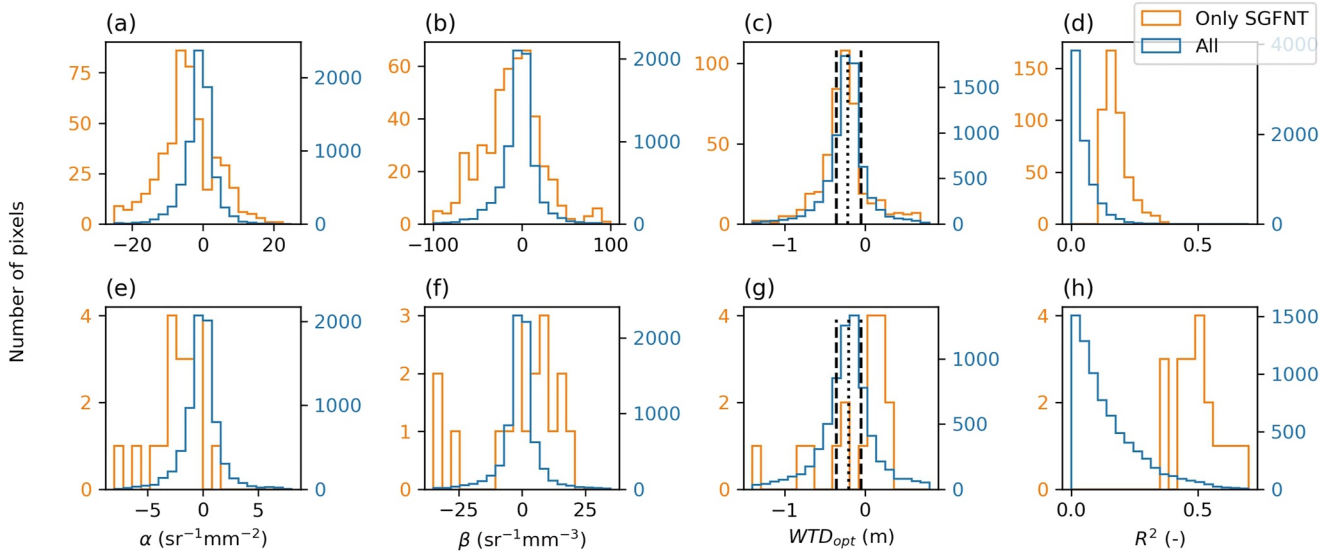


Figure 4. Histograms of α , β , WTD_{opt} and R^2 values for all pixels and pixels with significant (SGFNT) model fits for short-term anomalies (a–d) and long-term anomalies (e–h). R^2 refers to the coefficient of determination between observed and modeled $SIF_{n,anom}$. Dashed lines in panels (c) and (g) represent the median maximum water table depth (WTD) and the median minimum WTD of all pixels, dotted lines represent the median WTD_{opt} of all pixels.

influence of time-lag effects in long-term anomalies which our model does not account for. Unrealistic estimates of WTD_{opt} might also occur when optimal conditions have never been reached over the 4 years of data and therefore the β parameter was not sufficiently constrained. In general, R^2 values were larger for long-term anomalies than for short-term anomalies, but by correcting the sample size for temporal autocorrelation the number of significant pixels was less for the long-term compared to short-term analysis.

Figure 5 spatially shows the model-based estimates of the percentage of drought regime days per growing season from the SIF and the in situ GPP analysis. Dominant drought stress regimes were present for the short- and long-term analysis in the south of the Western Siberian Lowlands and the Boreal Plains. At those locations, peatlands are close to their climatic tolerance limits suggesting a higher probability of drought conditions (Devito

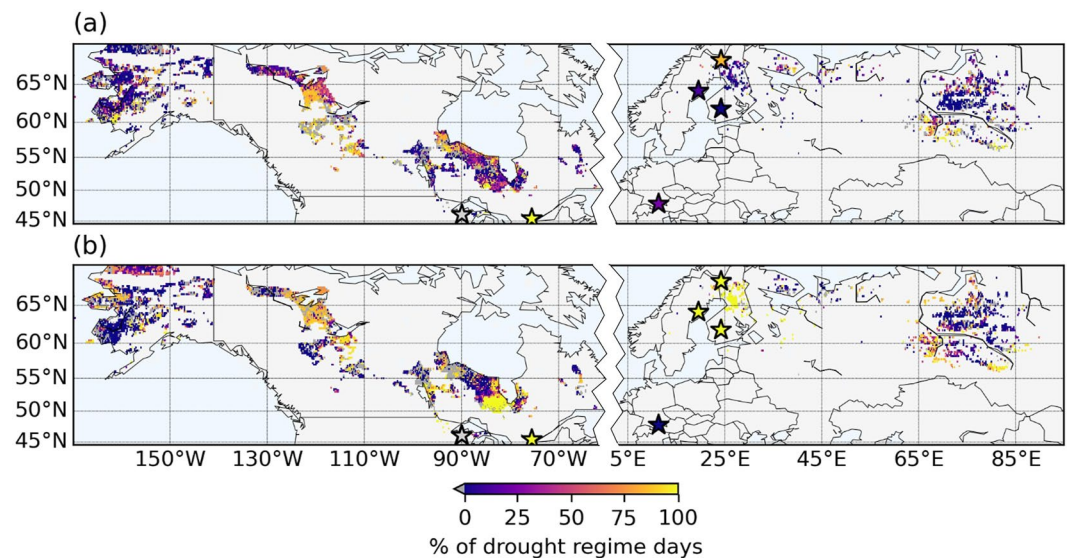


Figure 5. The percentage of days in a drought regime per growing season for (a) short-term anomalies and (b) long-term anomalies. The locations from the Eddy Covariance flux tower Gross Primary Production data are shown as stars. Pixels and stars for which WTD_{opt} was within the observed water table depth range but β was positive do not permit the calculation of drought regime days and are shown in dark gray.

et al., 2012; Gallego-Sala et al., 2018). The long-term analysis additionally identified a predominant drought stress regime in Finland which was not indicated in the short-term results. The same disagreement between short- and long-term results was observed for the three nearby EC flux tower sites and might be related to time-lag effects that are included in long-term but not in short-term anomalies (Lund et al., 2012).

4. Conclusion

The main novelty of this study is that not only drought but also waterlogging stress was identified in peatlands through SIF observations. Earlier studies on mineral soils identified either only drought stress or indirect impacts of flooding through delayed planting on agricultural fields (Helm et al., 2020; R. Qiu et al., 2022b; Yin et al., 2020; Zhang et al., 2019; Sun et al., 2015).

We identified water-related stress by using an anomaly based, peatland-specific WTD stress model, which builds upon laboratory fluorescence observations on *S. mosses* that indicated drought and waterlogging stress as a function of water table (Schipperges & Rydin, 1998). Our analysis was performed with either short- or long-term anomalies and revealed that the corresponding spatial median of optimal WTD, that is, minimum water-related stress, across all northern peatlands was -0.22 or -0.20 m, respectively, with only a small uncertainty of the spatial median of ± 0.01 m as indicated by bootstrap analysis. Our findings are in basic agreement with results from the same type of analysis of in situ GPP data. Future research should investigate the possible time-lagged impact of water-related stress on vegetation growth (Lund et al., 2012) that we likely observed in our long-term anomaly results.

The findings from our study could be used to evaluate and eventually constrain the water-related stress function in peatland-specific models (Mozafari et al., 2023). For instance, analyzing the output from peatland models with the proposed WTD stress model, as we did here with observations, could serve as a first insight into how well peatland models represent the characteristics of the observed stress response over peatlands. While reduced transpiration due to waterlogging stress has been recently added to a tropical peatland model (Apers et al., 2022), the effect on GPP has not been addressed yet and may help to better predict the feedback of peatlands to climate change (C. Qiu et al., 2022a).

Future research should also investigate the spatial pattern of the SIF-WTD relationship and how it depends on the vegetation type. Vascular vegetation tends to experience waterlogging stress already in less wet conditions than Sphagnum vegetation and may, to some extent, be more resilient to prolonged dry periods (Dimitrov et al., 2011; Harris et al., 2005). Upcoming higher spatial resolution SIF missions (e.g., the Fluorescence Explorer with an expected launch in 2025) may help to resolve the effect of vegetation type.

Data Availability Statement

TROPOMI SIF retrieval products are available for download from Koehler and Frankenberg (2020), CERES PAR data from NASA/LARC/SD/ASDC (2017), and modeled peatland WTD data from Bechtold et al. (2023). In situ GPP data is available at databases indicated in Table S1 in Supporting Information S1.

References

- AghaKouchak, A., Farahmand, A., Melton, F. S., Teixeira, J., Anderson, M. C., Wardlow, B. D., & Hain, C. R. (2015). Remote sensing of drought: Progress, challenges and opportunities. *Reviews of Geophysics*, 53(2), 452–480. <https://doi.org/10.1002/2014RG000456>
- Apers, S., De Lannoy, G. J. M., Baird, A. J., Cobb, A. R., Dargie, G. C., del Aguila Pasquel, J., et al. (2022). Tropical peatland hydrology simulated with a global land surface model. *Journal of Advances in Modeling Earth Systems*, 14(3), e2021MS002784. <https://doi.org/10.1029/2021MS002784>
- Baker, N. R. (2008). Chlorophyll fluorescence: A probe of photosynthesis in vivo. *Annual Review of Plant Biology*, 59(1), 89–113. <https://doi.org/10.1146/annurev.arplant.59.032607.092759>
- Bechtold, M., De Lannoy, G. J. M., Koster, R. D., Reichle, R. H., Mahanama, S. P., Bleuten, W., et al. (2019). PEAT-CLSM: A specific treatment of peatland hydrology in the NASA catchment land surface model. *Journal of Advances in Modeling Earth Systems*, 11(7), 2130–2162. <https://doi.org/10.1029/2018MS001574>
- Bechtold, M., De Lannoy, G. J. M., & Reichle, R. (2023). PEATCLSM(Tb): A land surface data assimilation product for peatlands using PEAT-CLSM and brightness temperature (Tb) satellite observations (Northern Hemisphere output, Jan 2010 through Sep 2021) [Dataset]. Zenodo. <https://doi.org/10.5281/ZENODO.8260830>
- Bechtold, M., De Lannoy, G. J. M., Reichle, R. H., Roose, D., Balliston, N., Burdun, I., et al. (2020). Improved groundwater table and L-band brightness temperature estimates for Northern Hemisphere peatlands using new model physics and SMOS observations in a global data assimilation framework. *Remote Sensing of Environment*, 246, 111805. <https://doi.org/10.1016/j.rse.2020.111805>

Acknowledgments

This research was funded by the Research Foundation Flanders (FWO, G095720N). The computer resources and services used in this work were provided by the High-Performance Computing system of the Vlaams Supercomputer Centrum, funded by FWO and the Flemish Government. D.G.M. acknowledges support from the European Research Council (ERC) under grant agreement 101088405 (HEAT). We acknowledge all funding agencies that supported the acquisition of long-term flux tower observations. We thank Ullrich Dettmann and Bäerbel Tiemeyer (both Thünen Institute) for providing water table data for DE_SFS to the European Fluxes Database.

- Brown, J. F., Wardlow, B. D., Tadesse, T., Hayes, M. J., & Reed, B. C. (2008). The vegetation drought response index (VegDRI): A new integrated approach for monitoring drought stress in vegetation. *GIScience and Remote Sensing*, 45(1), 16–46. <https://doi.org/10.2747/1548-1603.45.1.16>
- Burdun, I., Bechtold, M., Sagris, V., Lohila, A., Humphreys, E., Desai, A. R., et al. (2020). Satellite determination of peatland water table temporal dynamics by localizing representative pixels of a SWIR-based moisture index. *Remote Sensing*, 12(18), 2936. <https://doi.org/10.3390/rs12182936>
- Clymo, R. S., Turunen, J., & Tolonen, K. (1998). Carbon accumulation in Peatland. *Oikos*, 81(2), 368–388. <https://doi.org/10.2307/3547057>
- Dechant, B., Ryu, Y., Badgley, G., Köhler, P., Rascher, U., Migliavacca, M., et al. (2022). NIRVP: A robust structural proxy for sun-induced chlorophyll fluorescence and photosynthesis across scales. *Remote Sensing of Environment*, 268, 112763. <https://doi.org/10.1016/j.rse.2021.112763>
- Devito, K., Mendoza, C., & Qualizza, A. (2012). Conceptualizing water movement in the Boreal Plains. Implications for watershed reconstruction. *Environmental and Reclamation Research Group*, 164. <https://doi.org/10.7939/R32J4H>
- Dimitrov, D. D., Grant, R. F., Lafleur, P. M., & Humphreys, E. R. (2011). Modeling the effects of hydrology on gross primary productivity and net ecosystem productivity at Mer Bleue bog. *Journal of Geophysical Research*, 116(G4), G04010. <https://doi.org/10.1029/2010JG001586>
- Doelling, D. R., Loeb, N. G., Keyes, D. F., Nordeen, M. L., Morstad, D., Nguyen, C., et al. (2013). Geostationary enhanced temporal interpolation for CERES flux products. *Journal of Atmospheric and Oceanic Technology*, 30(6), 1072–1090. <https://doi.org/10.1175/JTECH-D-12-00136.1>
- Doelling, D. R., Sun, M., Nguyen, L. T., Nordeen, M. L., Haney, C. O., Keyes, D. F., & Mlynarczyk, P. E. (2016). Advances in geostationary-derived longwave fluxes for the CERES synoptic (SYN1deg) product. *Journal of Atmospheric and Oceanic Technology*, 33(3), 503–521. <https://doi.org/10.1175/JTECH-D-15-0147.1>
- Draper, C., & Reichle, R. (2015). The impact of near-surface soil moisture assimilation at subseasonal, seasonal, and inter-annual timescales. *Hydrology and Earth System Sciences*, 19(12), 4831–4844. <https://doi.org/10.5194/hess-19-4831-2015>
- Fenner, N., & Freeman, C. (2011). Drought-induced carbon loss in peatlands. *Nature Geoscience*, 4(12), 895–900. <https://doi.org/10.1038/ngeo1323>
- Frankenberg, C., Fisher, J. B., Worden, J., Badgley, G., Saatchi, S. S., Lee, J.-E., et al. (2011). New global observations of the terrestrial carbon cycle from GOSAT: Patterns of plant fluorescence with gross primary productivity. *Geophysical Research Letters*, 38(17), L17706. <https://doi.org/10.1029/2011GL048738>
- Gallego-Sala, A. V., Charman, D. J., Brewer, S., Page, S. E., Prentice, I. C., Friedlingstein, P., et al. (2018). Latitudinal limits to the predicted increase of the peatland carbon sink with warming. *Nature Climate Change*, 8(10), 907–913. <https://doi.org/10.1038/s41558-018-0271-1>
- Gruber, A., De Lannoy, G., Albergel, C., Al-Yaari, A., Brocca, L., Calvet, J.-C., et al. (2020). Validation practices for satellite soil moisture retrievals: What are (the) errors? *Remote Sensing of Environment*, 244, 111806. <https://doi.org/10.1016/j.rse.2020.111806>
- Gruber, A., & Reichle, R. H. (2022). Uncertainty estimation for SMAP Level-1 brightness temperature assimilation at different timescales. *Ieee Journal of Selected Topics in Applied Earth Observations and Remote Sensing*, 15, 9127–9145. <https://doi.org/10.1109/JSTARS.2022.3216213>
- Guanter, L., Bacour, C., Schneider, A., Aben, I., Van Kempen, T. A., Maignan, F., et al. (2021). The TROPISIF global sun-induced fluorescence dataset from the Sentinel-5P TROPOMI mission. *Earth System Science Data*, 13(11), 5423–5440. <https://doi.org/10.5194/essd-13-5423-2021>
- Guanter, L., Frankenberg, C., Dudhia, A., Lewis, P. E., Gómez-Dans, J., Kuze, A., et al. (2012). Retrieval and global assessment of terrestrial chlorophyll fluorescence from GOSAT space measurements. *Remote Sensing of Environment*, 121, 236–251. <https://doi.org/10.1016/j.rse.2012.02.006>
- Guanter, L., Zhang, Y., Jung, M., Joiner, J., Voigt, M., Berry, J. A., et al. (2014). Global and time-resolved monitoring of crop photosynthesis with chlorophyll fluorescence. *Proceedings of the National Academy of Sciences of the United States of America*, 111(14), E1327–E1333. <https://doi.org/10.1073/pnas.1320008111>
- Harris, A. (2008). Spectral reflectance and photosynthetic properties of Sphagnum mosses exposed to progressive drought. *Ecohydrology*, 1(1), 35–42. <https://doi.org/10.1002/eco.5>
- Harris, A., Bryant, R., & Baird, A. J. (2005). Detecting near-surface moisture stress in Sphagnum spp. *Remote Sensing of Environment*, 97(3), 371–381. <https://doi.org/10.1016/j.rse.2005.05.001>
- Helbig, M., Waddington, J. M., Alekseychik, P., Amiro, B. D., Aurela, M., Barr, A. G., et al. (2020). Increasing contribution of peatlands to boreal evapotranspiration in a warming climate. *Nature Climate Change*, 10(6), 555–560. <https://doi.org/10.1038/s41558-020-0763-7>
- Helm, L. T., Shi, H., Lerdau, M. T., & Yang, X. (2020). Solar-induced chlorophyll fluorescence and short-term photosynthetic response to drought. *Ecological Applications*, 30(5). <https://doi.org/10.1002/eap.2101>
- Ji, L., Zhang, L., & Wylie, B. (2009). Analysis of dynamic thresholds for the normalized difference water index. *Photogrammetric Engineering and Remote Sensing*, 75(11), 1307–1317. <https://doi.org/10.14358/PERS.75.11.1307>
- Jonard, F., De Cannière, S., Brüggemann, N., Gentine, P., Short Gianotti, D., Lobet, G., et al. (2020). Value of sun-induced chlorophyll fluorescence for quantifying hydrological states and fluxes: Current status and challenges. *Agricultural and Forest Meteorology*, 291, 108088. <https://doi.org/10.1016/j.agrformet.2020.108088>
- Joosten, H., & Clarke, D. (2002). *Wise use of mires and peatlands: Background and principles including a framework for decision-making*. International Peat Society; International Mire Conservation Group.
- Koehler, P., & Frankenberg, C. (2020). Ungridded TROPOMI SIF (at 740nm) [Dataset]. CaltechDATA. <https://doi.org/10.22002/D1.1347>
- Köhler, P., Frankenberg, C., Magney, T. S., Guanter, L., Joiner, J., & Landgraf, J. (2018). Global retrievals of solar-induced chlorophyll fluorescence with TROPOMI: First results and intersensor comparison to OCO-2. *Geophysical Research Letters*, 45(19), 10456–10463. <https://doi.org/10.1029/2018GL079031>
- Lees, K., Quaipe, T., Artz, R., Khomik, M., & Clark, J. (2018). Potential for using remote sensing to estimate carbon fluxes across northern peatlands—A review. *The Science of the Total Environment*, 615, 857–874. <https://doi.org/10.1016/j.scitotenv.2017.09.103>
- Limpens, J., Berendse, F., Blodau, C., Canadell, J. G., Freeman, C., Holden, J., et al. (2008). Peatlands and the carbon cycle: From local processes to global implications—A synthesis. *Biogeosciences*, 5(5), 1475–1491. <https://doi.org/10.5194/bg-5-1475-2008>
- Loisel, J., Gallego-Sala, A. V., Amesbury, M. J., Maignan, G., Anshari, G., Beilman, D. W., et al. (2021). Expert assessment of future vulnerability of the global peatland carbon sink. *Nature Climate Change*, 11(1), 70–77. <https://doi.org/10.1038/s41558-020-00944-0>
- Lund, M., Christensen, T. R., Lindroth, A., & Schubert, P. (2012). Effects of drought conditions on the carbon dioxide dynamics in a temperate peatland. *Environmental Research Letters*, 7(4), 045704. <https://doi.org/10.1088/1748-9326/7/4/045704>
- Martini, D., Sakowska, K., Wohlfahrt, G., Pacheco-Labrador, J., van der Tol, C., Porcar-Castell, A., et al. (2022). Heatwave breaks down the linearity between sun-induced fluorescence and gross primary production. *New Phytologist*, 233(6), 2415–2428. <https://doi.org/10.1111/nph.17920>
- Mohammed, G. H., Colombo, R., Middleton, E. M., Rascher, U., van der Tol, C., Nedbal, L., et al. (2019). Remote sensing of solar-induced chlorophyll fluorescence (SIF) in vegetation: 50 years of progress. *Remote Sensing of Environment*, 231, 111177. <https://doi.org/10.1016/j.rse.2019.04.030>
- Moore, P. D. (2002). The future of cool temperate bogs. *Environmental Conservation*, 29(1), 3–20. <https://doi.org/10.1017/S0376892902000024>

- Mozafari, B., Bruen, M., Donohue, S., Renou-Wilson, F., & O'Loughlin, F. (2023). Peatland dynamics: A review of process-based models and approaches. *The Science of the Total Environment*, 877, 162890. <https://doi.org/10.1016/j.scitotenv.2023.162890>
- Nanzad, L., Zhang, J., Tuvdendorj, B., Nabil, M., Zhang, S., & Bai, Y. (2019). NDVI anomaly for drought monitoring and its correlation with climate factors over Mongolia from 2000 to 2016. *Journal of Arid Environments*, 164, 69–77. <https://doi.org/10.1016/j.jaridenv.2019.01.019>
- NASA/LARC/SD/ASDC. (2017). CERES and GEO-enhanced TOA, within-atmosphere and surface fluxes, clouds and aerosols 3-hourly Terra-Aqua Edition4A [Dataset]. NASA Langley Atmospheric Science Data Center Distributed Active Archive Center DAAC. https://doi.org/10.5067/TERRA+AQUA/CERES/SYN1DEG-3HOUR_L3.004A
- Panigada, C., Rossini, M., Meroni, M., Cilia, C., Busetto, L., Amaducci, S., et al. (2014). Fluorescence, PRI and canopy temperature for water stress detection in cereal crops. *International Journal of Applied Earth Observation and Geoinformation*, 30(1), 167–178. <https://doi.org/10.1016/j.jag.2014.02.002>
- Qiu, C., Ciaia, P., Zhu, D., Guenet, B., Chang, J., Chaudhary, N., et al. (2022a). A strong mitigation scenario maintains climate neutrality of northern peatlands. *One Earth*, 5(1), 86–97. <https://doi.org/10.1016/j.oneear.2021.12.008>
- Qiu, R., Li, X., Han, G., Xiao, J., Ma, X., & Gong, W. (2022b). Monitoring drought impacts on crop productivity of the U.S. Midwest with solar-induced fluorescence: GOSIF outperforms GOME-2 SIF and MODIS NDVI, EVI, and NIRv. *Agricultural and Forest Meteorology*, 323, 109038. <https://doi.org/10.1016/j.agrformet.2022.109038>
- Reichle, R. H., Liu, Q., Ardizzone, J. V., Bechtold, M., Crow, W. T., Lannoy, G. J. M. D., et al. (2023). In *Soil moisture active passive (SMAP) project assessment report for version 7 of the 14_sm data product, NASA technical report series on global modeling and data assimilation, nasa/tm-2023-104606* (Vol. 64, p. 87). National Aeronautics and Space Administration, Goddard Space Flight Center.
- Rinne, J., Tuovinen, J. P., Klemetsson, L., Aurela, M., Holst, J., Lohila, A., et al. (2020). Effect of the 2018 European drought on methane and carbon dioxide exchange of northern mire ecosystems: 2018 drought on northern mires. *Philosophical Transactions of the Royal Society B: Biological Sciences*, 375(1810), 20190517. <https://doi.org/10.1098/rstb.2019.0517>
- Robroek, B. J. M., Schouten, M. G. C., Limpens, J., Berendse, F., & Poorter, H. (2009). Interactive effects of water table and precipitation on net CO₂ assimilation of three co-occurring *Sphagnum* mosses differing in distribution above the water table. *Global Change Biology*, 15(3), 680–691. <https://doi.org/10.1111/j.1365-2486.2008.01724.x>
- Schipperges, B., & Rydin, H. (1998). Response of photosynthesis of *Sphagnum* species from contrasting microhabitats to tissue water content and repeated desiccation. *New Phytologist*, 140(4), 677–684. <https://doi.org/10.1046/j.1469-8137.1998.00311.x>
- Sun, Y., Frankenberg, C., Wood, J. D., Schimel, D. S., Jung, M., Guanter, L., et al. (2017). OCO-2 advances photosynthesis observation from space via solar-induced chlorophyll fluorescence. *Science*, 358(6360), eaam5747. <https://doi.org/10.1126/science.aam5747>
- Sun, Y., Fu, R., Dickinson, R., Joiner, J., Frankenberg, C., Gu, L., et al. (2015). Drought onset mechanisms revealed by satellite solar-induced chlorophyll fluorescence: Insights from two contrasting extreme events. *Journal of Geophysical Research: Biogeosciences*, 120(11), 2427–2440. <https://doi.org/10.1002/2015JG003150>
- Tian, F., Wu, J., Liu, L., Leng, S., Yang, J., Zhao, W., & Shen, Q. (2019). Exceptional drought across Southeastern Australia caused by extreme lack of precipitation and its impacts on NDVI and SIF in 2018. *Remote Sensing*, 12(1), 54. <https://doi.org/10.3390/rs12010054>
- Van Gaalen, K. E., Flanagan, L. B., & Peddle, D. R. (2007). Photosynthesis, chlorophyll fluorescence and spectral reflectance in *Sphagnum* moss at varying water contents. *Oecologia*, 153(1), 19–28. <https://doi.org/10.1007/s00442-007-0718-y>
- Waddington, J. M., Morris, P. J., Kettridge, N., Granath, G., Thompson, D. K., & Moore, P. A. (2014). Hydrological feedbacks in northern peatlands. *Ecohydrology*, 8(1), 113–127. <https://doi.org/10.1002/eco.1493>
- Walther, S., Guanter, L., Heim, B., Jung, M., Duveiller, G., Wolanin, A., & Sachs, T. (2018). Assessing the dynamics of vegetation productivity in circumpolar regions with different satellite indicators of greenness and photosynthesis. *Biogeosciences*, 15(20), 6221–6256. <https://doi.org/10.5194/bg-15-6221-2018>
- Wang, Y., Zeng, Y., Yu, L., Yang, P., Van Der Tol, C., Yu, Q., et al. (2021). Integrated modeling of canopy photosynthesis, fluorescence, and the transfer of energy, mass, and momentum in the soil-plant-Atmosphere continuum (STEMMUS-SCOPE v1.0.0). *Geoscientific Model Development*, 14(3), 1379–1407. <https://doi.org/10.5194/gmd-14-1379-2021>
- Wardlow, B. D., Anderson, M. C., & Verdin, J. P. (Eds.) (2012). *Remote sensing of drought: Innovative monitoring approaches*. CRC Press.
- Wieneke, S., Burkart, A., Cendrero-Mateo, M., Julitta, T., Rossini, M., Schickling, A., et al. (2018). Linking photosynthesis and sun-induced fluorescence at sub-daily to seasonal scales. *Remote Sensing of Environment*, 219, 247–258. <https://doi.org/10.1016/j.rse.2018.10.019>
- Worrall, F., Boothroyd, I. M., Gardner, R. L., Howden, N. J. K., Burt, T. P., Smith, R., et al. (2019). The impact of peatland restoration on local climate: Restoration of a cool Humid Island. *Journal of Geophysical Research: Biogeosciences*, 124(6), 1696–1713. <https://doi.org/10.1029/2019JG005156>
- Yin, Y., Byrne, B., Liu, J., Wennberg, P. O., Davis, K. J., Magney, T., et al. (2020). Cropland carbon uptake delayed and reduced by 2019 Midwest floods. *AGU Advances*, 1(1). <https://doi.org/10.1029/2019AV000140>
- Zhang, L., Qiao, N., Huang, C., & Wang, S. (2019). Monitoring drought effects on vegetation productivity using satellite solar-induced chlorophyll fluorescence. *Remote Sensing*, 11(4), 378. <https://doi.org/10.3390/rs11040378>

References From the Supporting Information

- Aurela, M., Lohila, A., Tuovinen, J. P., Hatakka, J., Penttilä, T., & Laurila, T. (2015). Carbon dioxide and energy flux measurements in four northern-boreal ecosystems at Pallas. *Boreal Environment Research*, 20(4), 455–473.
- Aurela, M., Lohila, A., Tuovinen, J. P., Hatakka, J., Riutta, T., & Laurila, T. (2009). Carbon dioxide exchange on a northern boreal fen. *Boreal Environment Research*, 14(4), 699–710. <https://doi.org/10.1093/treephys/tpn047>
- Desai, A. R. (2023). AmeriFlux BASE US-LOS Lost Creek, ver. 25-5, AmeriFlux AMP [Dataset]. AmeriFlux AMP. <https://doi.org/10.17190/AMF/1246071>
- Dettmann, U., & Bechtold, M. (2016). Deriving effective soil water retention characteristics from shallow water table fluctuations in Peatlands. *Vadose Zone Journal*, 15(10), 1–13. <https://doi.org/10.2136/vzj2016.04.0029>
- Hommeltenberg, J., Mauder, M., Drösler, M., Heidbach, K., Werle, P., & Schmid, H. P. (2014). Ecosystem scale methane fluxes in a natural temperate bog-pine forest in southern Germany. *Agricultural and Forest Meteorology*, 198, 273–284. <https://doi.org/10.1016/j.agrformet.2014.08.017>
- Lafleur, P. M., Hember, R. A., Admiral, S. W., & Roulet, N. T. (2005). Annual and seasonal variability in evapotranspiration and water table at a shrub-covered bog in southern Ontario, Canada. *Hydrological Processes*, 19(18), 3533–3550. <https://doi.org/10.1002/hyp.5842>
- Nilsson, M., Sagerfors, J., Buffam, I., Laudon, H., Eriksson, T., Grelle, A., et al. (2008). Contemporary carbon accumulation in a boreal oligotrophic minerogenic mire—A significant sink after accounting for all C-fluxes. *Global Change Biology*, 14(10), 2317–2332. <https://doi.org/10.1111/j.1365-2486.2008.01654.x>

- Peichl, M., Sagerfors, J., Lindroth, A., Buffam, I., Grelle, A., Klemetsson, L., et al. (2013). Energy exchange and water budget partitioning in a boreal minerogenic mire. *Journal of Geophysical Research: Biogeosciences*, *118*(1), 1–13. <https://doi.org/10.1029/2012JG002073>
- Rinne, J., Tuittila, E. S., Peltola, O., Li, X., Raivonen, M., Alekseychik, P., et al. (2018). Temporal variation of ecosystem scale methane emission from a boreal fen in relation to temperature, water table position, and carbon dioxide fluxes. *Global Biogeochemical Cycles*, *32*(7), 1087–1106. <https://doi.org/10.1029/2017GB005747>
- Riutta, T., Laine, J., Aurela, M., Rinne, J., Vesala, T., Laurila, T., et al. (2007). Spatial variation in plant community functions regulates carbon gas dynamics in a boreal fen ecosystem. *Tellus B: Chemical and Physical Meteorology*, *59*(5). <https://doi.org/10.3402/tellusb.v59i5.17063>
- Sulman, B. N., Desai, A. R., Cook, B. D., Saliendra, N., & MacKay, D. S. (2009). Contrasting carbon dioxide fluxes between a drying shrub wetland in Northern Wisconsin, USA, and nearby forests. *Biogeosciences*, *6*(6), 1115–1126. <https://doi.org/10.5194/bg-6-1115-2009>